

1           **Associations of interannual variation of Summer Tropospheric Ozone with**  
2           **Western Pacific Subtropical High in China from 1999 to 2017**

3  
4   **Authors:** Xiaodong Zhang<sup>1,#</sup>, Ruiyu Zhugu<sup>1,#</sup>, Xiaohu Jian<sup>1</sup>, Xinrui Liu<sup>1</sup>, Kaijie Chen<sup>1</sup>,  
5   Shu Tao<sup>1</sup>, Junfeng Liu<sup>1</sup>, Hong Gao<sup>2</sup>, Tao Huang<sup>2</sup>, Jianmin Ma<sup>1,\*</sup>

6  
7   **Affiliations:**

8   <sup>1</sup>Laboratory for Earth Surface Processes, College of Urban and Environmental Sciences,  
9   Peking University, Beijing 100871, China

10   <sup>2</sup>Key Laboratory for Environmental Pollution Prediction and Control, College of Earth  
11   and Environmental Sciences, Lanzhou University, Lanzhou 730000, China

12  
13   # These authors contribute equally to this article

14   \* Corresponding author. E-mail address: [jmma@pku.edu.cn](mailto:jmma@pku.edu.cn) (J.M. Ma).

15  
16   **Abstract**

17   Associations between tropospheric ozone (O<sub>3</sub>) and climate variations have been  
18   extensively investigated worldwide. However, given the lack of historical O<sub>3</sub>  
19   monitoring data, the knowledge gaps regarding the influences of climate variations on  
20   long-term O<sub>3</sub> trends in China remain. The present study used a ~~unique~~ tropospheric O<sub>3</sub>  
21   dataset from the summer of 1999 to 2017 simulated by an atmospheric chemistry model  
22   to explore the linkage between summer O<sub>3</sub> and a dominant atmospheric circulation  
23   system – the Western Pacific Subtropical High Pressure (WPSH) on an interannual  
24   basis in China. During this period, both WPSH strength and O<sub>3</sub> concentrations in  
25   eastern and central China illustrated a growing trend. An EOF analysis was conducted  
26   to examine significant summer O<sub>3</sub> characteristics and patterns and their potential  
27   connections with the WPSH. We find that the correlation between first principal  
28   component of summer ozone concentration in the EOF analysis and the WPSH reached  
29   0.56 ( $P \leq 0.01$ ) in China from 1999 to 2017. We show that the WPSH determines  
30   interannual fluctuations of summer O<sub>3</sub>, whereas O<sub>3</sub> precursor emissions contribute  
31   primarily to the O<sub>3</sub> long-term trend. ~~Special efforts were made to discern the~~

~~associations of O<sub>3</sub> variations in major urban agglomerations of China and the WPSH.~~  
The Our results reveal that the WPSH plays a ~~more~~ vital role in O<sub>3</sub> perturbation in the eastern seaboard regions and inland China, ~~but leads to lower O<sub>3</sub> levels in the Pearl River Delta (PRD) region.~~ Precursor emissions made more significant contributions up to 60% to increasing O<sub>3</sub> trends in the inland urban agglomerations than coastal regions in eastern and southern China. The strongest contribution of meteorological conditions associated with the WPSH to summer ~~ozone concentration~~ O<sub>3</sub> occurred in the Yangtze River Delta (YRD), accounting for over 9% to ozone perturbations from 1999 to 2017. ~~Overall, we~~ We find that the effect of the WPSH on regional O<sub>3</sub> depends on the spatial proximity to the WPSH. We attributed the effects of the WPSH on O<sub>3</sub> interannual variations to the changes in air temperature, precipitation, and winds associated with the WPSH's intensity and positions. –

**Keywords:** tropospheric ozone, western pacific subtropical high, climate, EOF analysis

## 1. Introduction

Tropospheric (or surface) ozone is one of the most important components of atmospheric chemistry and is also a prominent atmospheric pollutant in China in recent years (Ma et al., 2021). Ground-level ozone pollution has overtaken PM<sub>2.5</sub> as the leading pollutant in many of China's urban and industrial regions (Lu et al., 2018). Surface ozone is produced through the photochemical oxidation of carbon monoxide (CO) and volatile organic compounds (VOCs) in the presence of nitrogen oxides (NO<sub>x</sub>) and sunlight (Akimoto et al., 2015; Liu and Wang, 2020; Lu et al., 2018; Ma et al., 2021). Unlike stratospheric ozone, which absorbs harmful UV radiation that could otherwise reach the Earth's surface and cause adverse health impacts on humans, surface ozone has detrimental effects on both human health and terrestrial vegetation (Brauer et al., 2012; ~~(~~Fleming et al., 2018; Lefohn et al., 2017; Liu et al., 2018; Liu and Wang, 2020). ~~Extensive studies have revealed significant associations between short-term or acute exposure to ozone concentrations and respiratory and cardiovascular~~

60 ~~morbidity, inhibiting lung development, new onset asthma, hospital admissions, and~~  
61 ~~premature mortality (Bell et al., 2014; Fleming et al., 2018; Yan et al., 2013). It is~~  
62 ~~estimated that death related to ozone exposure comprises 5–20% of all those caused by~~  
63 ~~air pollution (Brauer et al., 2012; Monks et al., 2015; Silva et al., 2013). In the past~~  
64 decade, partly due to rapid economic growth and urbanization in China, surface O<sub>3</sub> has  
65 increased dramatically (Maji et al., 2019; Zhan et al., 2018). Many urban areas across  
66 China have experienced growing ozone pollution, despite implementing various  
67 stringent emission reduction measures since 2013 (Bell et al., 2014; Liu and Wang,  
68 2020; ~~Yan et al., 2013~~)Ma et al., 2016; Xu et al., 2016; Yan et al., 2013). ~~Although the~~  
69 ~~median ozone values exhibit no significant disparity between China and many~~  
70 ~~industrialized countries and regions such as Japan, South Korea, Europe, and the United~~  
71 ~~States (US), the frequency of high ozone events in China is much higher than those~~  
72 ~~developed countries and regions (Lu et al., 2018; Ma et al., 2016; Xu et al., 2016).~~

73 Surface ozone formation and evolution rely on meteorology, atmospheric  
74 chemistry, and the emissions of O<sub>3</sub> precursors, such as VOCs and NO<sub>x</sub> emitted from  
75 fuel combustion (Li et al., 2020; Ma et al., 2021). Meteorological parameters affecting  
76 surface O<sub>3</sub> evolution include but are not limited to winds, air temperature, relative  
77 humidity, and solar radiation (Ma et al., 2021). While anthropogenic factors play vital  
78 roles in ozone formation, meteorological factors determine, to a significant extent, the  
79 changes and evolution in O<sub>3</sub> concentrations (Ding et al., 2019; Li et al., 2019, 2020; Lin  
80 et al., 2021, 2022). Meteorological conditions modulate O<sub>3</sub> concentrations through  
81 atmospheric transport and affect natural emissions from biological sources and  
82 chemical reaction rates (Fu et al., 2019; Li et al., 2020; Lu et al., 2019). Extensive  
83 investigations have been devoted to short-term, such as hourly and diurnal changes in  
84 O<sub>3</sub> levels and their associations with meteorological conditions (Dang et al., 2021; Han  
85 et al., 2020). Given the strong connections between O<sub>3</sub> concentration and air  
86 temperature, atmospheric humidity, and winds, interannual and longer-term variations  
87 of O<sub>3</sub> are also elucidated in China and worldwide (Chen et al., 2020; Li et al., 2020).  
88 Daily and interannual variations of summertime surface O<sub>3</sub> have been linked with  
89 atmospheric teleconnection patterns, such as the ENSO (El Niño-Southern Oscillation),

90 East Asian summer monsoon, and the WPSH (Liu et al., 2019a; Wang et al., 2016;  
91 Yang et al., 2022; Yihui and Chan, 2005; Yin et al., 2019; Zhao and Wang, 2017; Zhou  
92 et al., 2009). These climate teleconnection patterns provide dynamic and  
93 thermodynamic backgrounds of regional and large-scale weather systems that could  
94 markedly affect the atmospheric pressure, temperature, and winds. Using modeled  
95 summer O<sub>3</sub> time series across China from 1999 to 2017, we have examined the response  
96 of gridded summer O<sub>3</sub> concentrations to the East Asian Summer Monsoon Index  
97 (EASMI), Nino indices, and western North Pacific subtropical high index (WPSH-I),  
98 the three climate modes influencing significantly the summer weather and climate in  
99 China, on an annual basis in the six major ~~urban agglomerations in China~~ (UAs, in  
100 China (Zhang, et al., 2022). The correlation coefficients between the summer O<sub>3</sub>  
101 concentrations and the three climate modes from 1999 to 2017 are 0.54 (WPSH-I,  
102 p=0.016), 0.38 (Nino indices, p=0.105), and 0.27 (EASMI, p=0.267), respectively. The  
103 results revealed that interannual changes in summer O<sub>3</sub> ~~in~~ averaged over these UAs were  
104 more significantly associated with the WPSH-I among ~~these three~~ atmospheric  
105 teleconnection patterns. The finding motivates us to carry out more broad and deep  
106 investigations of the associations between the long-term change in summer O<sub>3</sub> and the  
107 WPSH, aiming to shed new light on the extent of the impact of climate variation on O<sub>3</sub>  
108 trends in urban China.

109 Limited studies have been carried out to examine the linkage of summer O<sub>3</sub> in  
110 China with the WPSH (Jiang et al., 2021; Yin et al., 2019; Zhao and Wang, 2017; Liu  
111 et al., 2019a). These studies all focused on the response of daily and short-term summer  
112 O<sub>3</sub> variation to the WPSH in eastern China using measured O<sub>3</sub> concentrations within a  
113 short period (e.g., 2015-2018, Yin et al., 2019) ~~rather than interannual or longer ozone~~  
114 ~~trends in mainland China.~~ The common conclusions of these studies were that stronger  
115 WPSH tended to increase daily surface ozone concentration over northern China but  
116 reduce it over southern China, which was partly attributed to a stronger southwesterly  
117 transport of moisture into Southern China that was not conducive to ozone formation.  
118 However, the associations between interannual or longer-term variations of WPSH and  
119 interannual or longer ozone trends in mainland China are almost unknown. To fill this

120 knowledge gap, we performed multiple atmospheric chemistry model simulations of  
121 summer (June, July, and August) O<sub>3</sub> concentrations across China from 1999 to 2017.  
122 This ~~unique~~-O<sub>3</sub> dataset enables us to explore the responses of the long-term trend and  
123 interannual variation of O<sub>3</sub> concentrations to climate variations and to take a broader  
124 look at the associations between ozone evolution and the Western Pacific subtropical  
125 high in China (Zhang et al., 2022).

## 126 **2. Methodology**

### 127 **2.1. WRF-Chem Model Configuration**

128 The Weather Research and Forecasting model coupled with Chemistry (WRF-  
129 Chem) v3.7 ([http://www2.mmm.ucar.edu/wrf/users/wrf\\_files/wrfv3.7/updates-](http://www2.mmm.ucar.edu/wrf/users/wrf_files/wrfv3.7/updates-3.7.html)  
130 [3.7.html](http://www2.mmm.ucar.edu/wrf/users/wrf_files/wrfv3.7/updates-3.7.html)) was employed to quantify the influences of the WPSH on O<sub>3</sub> variation in  
131 China. The model covers mainland China with a 20 km × 20 km grid resolution,  
132 extending from the ground surface to 50 hPa with 30 non-uniformly distributed  
133 ~~verticle~~vertical layers (Zhang et al., 2022). Anthropogenic emissions data of  
134 atmospheric pollutants from 1998 to 2017 were collected from EDGAR (Emissions  
135 Database for Global Atmospheric Research) v4.3 (<https://edgar.jrc.ec.europa.eu/>),  
136 including gridded annual emission data for CH<sub>4</sub>, BC, OC, NH<sub>3</sub>, NMVOC, NO<sub>x</sub>, CO,  
137 SO<sub>2</sub>, and primary PM<sub>10</sub> and PM<sub>2.5</sub>. The biogenic emissions were estimated by the  
138 MEGAN v2.1 (Model of Emissions of Gases and Aerosols from Nature) (Guenther et  
139 al., 2012). Detailed WRF-Chem configuration, modeling setup, and precursor  
140 emissions are referred to by Zhang et al. (2022). WRF-Chem model was integrated to  
141 predict daily O<sub>3</sub> concentrations in summer (June to August) from 1998 to 2017. After  
142 excluding the model spin-up time, the O<sub>3</sub> time series from 1999 to 2017 was used in  
143 the present study. The daily concentrations were summed and averaged over the  
144 summer season to obtain mean O<sub>3</sub> concentrations. The modeled O<sub>3</sub> concentrations were  
145 verified by measured daily O<sub>3</sub> concentration data in several major ~~urban~~  
146 ~~agglomerations~~UAs across China. More details from 2016 to 2017. The results show

147 better agreements between modeled and sampled O<sub>3</sub> air concentrations. Details are  
148 referred to in Supporting Information Text 1-~~and~~, Fig. S1- and Zhang et al (2022).

## 149 **2.2. WPSH index**

150 The WPSH is an anticyclonic system hovering over the middle and lower  
151 troposphere of the northwestern Pacific Ocean. The WPSH forms during the summer  
152 months and dissipates in winter. As a high-pressure system, the WPSH is associated  
153 with stable weather conditions featured by high temperature and low rainfall. These  
154 weather conditions, in turn, perturb significantly O<sub>3</sub> variation. While varying year from  
155 year, the WPSH in summer generally covers much of East Asia, including parts of  
156 China, Japan, and the Korean Peninsula. It can also extend westward, affecting  
157 Southeast Asia, including Vietnam, Thailand, and the Philippines (Jiang et al., 2021;  
158 Yang et al., 2022). Although the summer WPSH determines primarily the weather and  
159 climate conditions in Eastern and Southern China, it may also influence the weather  
160 systems in Western and Northern China. For example, the westward and northward  
161 movement of the WPSH might lead to a weak high-pressure system in Northern  
162 Xinjiang extending to Central-North China, resulting in higher temperatures and lower  
163 rainfall in this region, whereas a low-pressure system could prevail in Northern and  
164 Northeastern China, enhancing precipitation in this part of China. However, given  
165 lower O<sub>3</sub> levels in Westernmost China (Tibet and Xinjiang), the present study did not  
166 attempt to elucidate the associations between O<sub>3</sub> evolution and the WPSH in this part  
167 of China but focused on Central and Eastern China where significantly higher O<sub>3</sub> levels  
168 were observed.

169 The WPSH indices were collected from the National Climate Center of China  
170 (NCCC, the WPSH index is available at [http://cmdp.ncc-](http://cmdp.ncc-cma.net/download/precipitation/diagnosis/NWP_high/wpsh_idx.txt)  
171 [cma.net/download/precipitation/diagnosis/NWP\\_high/wpsh\\_idx.txt](http://cmdp.ncc-cma.net/download/precipitation/diagnosis/NWP_high/wpsh_idx.txt)). The NCCC  
172 reports four WPSH indices, including the WPSH area index, intensity index, the  
173 westernmost point, and the ridgeline index of the WPSH. These indices define and  
174 quantify the changes in the WPSH via its size, intensity, east–west expansion, and

175 north–south movement (Liu et al., 2019b). These WPSH activities significantly affect  
176 China's daily, seasonal, interannual, and longer-term meteorological fields and climate  
177 variations. Among the four WPSH indices, we found that the WPSH area index  
178 (hereafter referred to as WPSH-I1) exhibited the most significant positive correlations  
179 with modeled summer ozone concentrations in most regions of China. ~~The strongest~~  
180 ~~negative correlations occur between O<sub>3</sub> concentrations and the westernmost point of the~~  
181 ~~WPSH (hereafter referred to as WPSH-I2).~~ Since summer rainfall in China was reported  
182 to be more sensitive to the western ridge point of the WPSH (Jiang et al., 2021; Yang  
183 et al., 2022; Zhao and Wang, 2017), which might affect the O<sub>3</sub> wet deposition, we also  
184 considered the westernmost point of the WPSH (hereafter referred to as WPSH-I2) in  
185 the present study. We found the strongest negative correlations between O<sub>3</sub>  
186 concentrations and WPSH-I2, which is likely associated with O<sub>3</sub> washout by  
187 precipitation. In light of this, we chose the WPSH-I1 and WPSH-I2 to elucidate the  
188 potential influences of the WPSH on the interannual variations of WRF-Chem  
189 simulated summer O<sub>3</sub> concentrations for the past two decades. As shown in **Fig. S2**, the  
190 WPSH strength characterized by the WPSH-I1 index illustrates a growing trend after  
191 1999, suggesting the reinforcement of the WPSH on a decadal scale in the recent two  
192 decades, the period coincident with the most rapidly growing O<sub>3</sub> pollution in China.  
193 This growth trend of the WPSH possibly overwhelms interannual changes in the WPSH  
194 ~~in the recent two decades.~~

### 195 **2.3. O<sub>3</sub> and meteorological data**

196 Surface O<sub>3</sub> concentration data on a daily basis used the WRF-Chem simulated  
197 concentration data (section 2.1). Meteorological data used the WRF predicted gridded  
198 air temperature (C°), 500-hPa geopotential height (GH, ghm), winds (m s<sup>-1</sup>), ~~and~~ the sea  
199 surface pressure (SSP, hPa-), and incoming solar radiation flux (W m<sup>-2</sup>). To  
200 ~~perform~~ reduce uncertainties from WRF predicted meteorological data in the composite  
201 analysis for examining the responses of interannual variation of summer ozone to the  
202 WPSH, we also collected NCEP reanalysis data based on meteorological observations,

203 including geopotential height at the 500 hPa, the surface air temperature (SAT, °C), and  
204 precipitation from NCEP reanalysis  
205 (<https://psl.noaa.gov/data/reanalysis/reanalysis.shtml>). These data were used to  
206 illustrate the characteristics of meteorological fields during the positive and negative  
207 phases of WPSH indices and in the first EOF loadings, which will be elaborated on  
208 below.

#### 209 **2.4. EOF analysis**

210 To extract the potential influences of the interannual changes in the WPSH on O<sub>3</sub>  
211 variations, we conducted the EOF analysis and examined associations between  
212 meteorological fields and surface O<sub>3</sub> from 1999 to 2017, ~~respectively~~. The empirical  
213 orthogonal function (EOF) analysis as a multivariate statistical technique has been  
214 extensively used in atmospheric science to explore the spatiotemporal variations in a  
215 meteorological variable or air pollutant (Fiore et al., 2003; Pu et al., 2016; Shen et al.,  
216 2015; Yin et al., 2019; Zhao and Wang, 2017). In the present study, we used the EOF  
217 analysis in WRF-Chem simulated gridded (20 km × 20 km) seasonal O<sub>3</sub> concentrations  
218 across China to extract annual O<sub>3</sub> change features from 1999 to 2017, ~~respectively~~. The  
219 EOF analysis of the O<sub>3</sub> concentration time series from modeled data was designed to  
220 investigate potential associations between the summer O<sub>3</sub> time series and WPSH and  
221 to explore the response of the O<sub>3</sub> time series to increasing WPSH strength since 1999.  
222 The orthogonal modes included spatial and temporal coefficients and contained  
223 information of some proportion (variance contributions) from the original fields.

#### 224 **2.5. Model scenario setup**

225 We quantify the contribution of meteorology and precursor emissions to O<sub>3</sub>  
226 evolution subject to WPSH by setting up three model scenarios. Considering the  
227 increasing trend of the WPSH from 1999 onward, we integrated WRF-Chem from 1998  
228 to 2017, subject to three model runs. The first model scenario run took the variable  
229 meteorological field and annual O<sub>3</sub> precursor emissions from 1998 to 2017, with 1998



230 as the model spin-up period, referred to as the base scenario (scenario 1); the second  
231 scenario run adopted fixed precursor emissions in 1998, but variable meteorology  
232 throughout 1998 to 2017, referred to as model scenario 2, and the third scenario  
233 implemented fixed meteorology in 1998 but variable precursor emissions, referred to  
234 as model scenario 3. The simulated O<sub>3</sub> concentrations from these three scenarios were  
235 compared to identify the relative significance of meteorology and precursor emissions  
236 in the changes in O<sub>3</sub> concentrations.

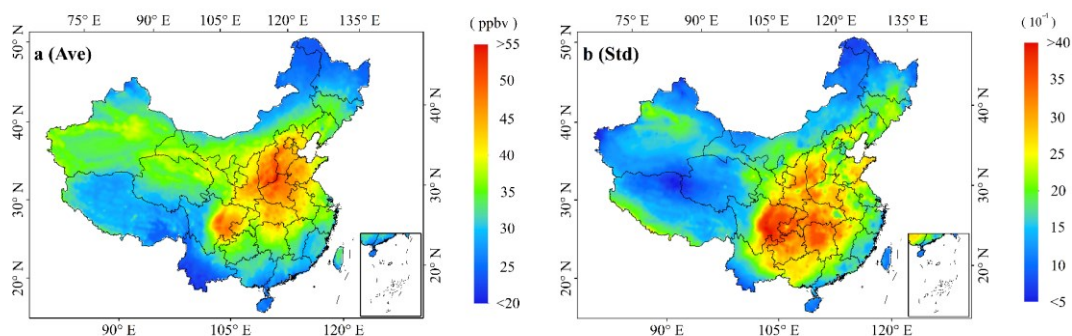
237

### 238 3. Results and Discussion

#### 239 3.1. EOF analysis

240 **Figures 1a** and **1b** show modeled summer mean O<sub>3</sub> concentrations and standard  
241 deviations (STD) averaged from 1999 to 2017. Higher concentrations are observed in  
242 Sichuan and the region extending from central China to the Northern China Plain (NCP),  
243 rather than the southern and southeastern seaboard areas where O<sub>3</sub> pollution has been  
244 receiving extensive concerns (**Fig. 1a**). This spatial distribution pattern agrees well with  
245 measured mean summer concentrations data averaged from 2015 to 2017 in China (**Fig.**  
246 **S3**). The STD distribution does not superimpose with O<sub>3</sub> concentrations but is centered  
247 in the Sichuan Basin and those provinces in the middle reaches of the Yangtze River,  
248 implying that O<sub>3</sub> fluctuated more strongly by interannual variations of meteorological  
249 fields in this region.

250



251

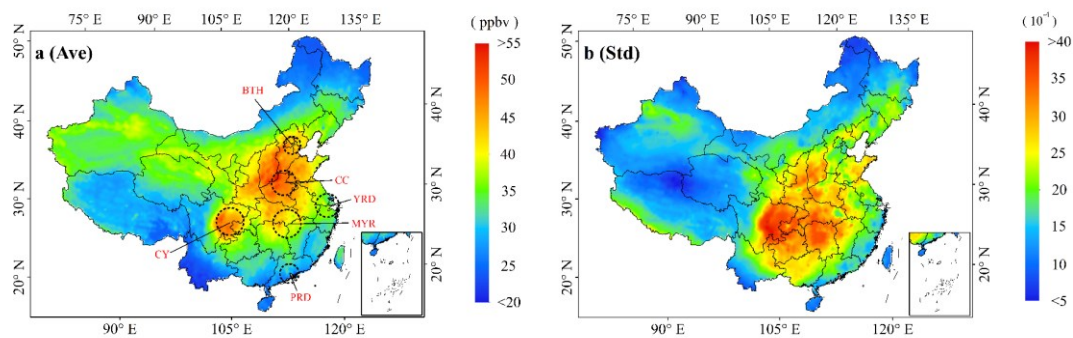
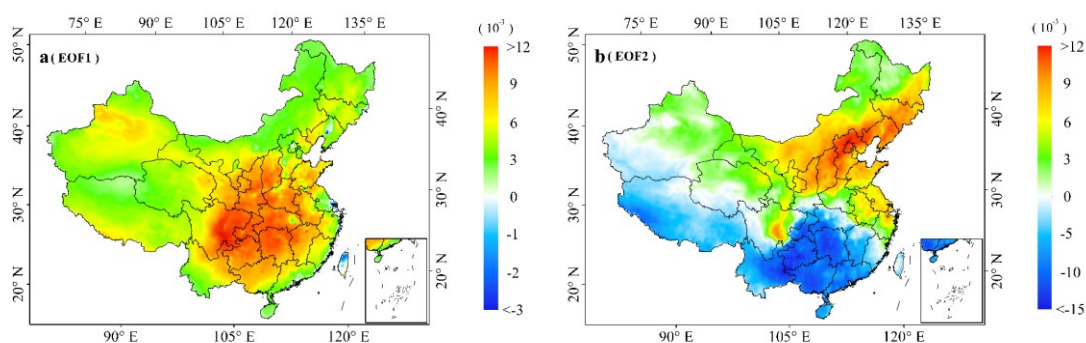


**Figure 1.** Mean summer O<sub>3</sub> concentrations **(a)** and standard deviations **(b)** averaged from 1999 to 2017.

We carried out an EOF analysis by using summer O<sub>3</sub> as the original field to illustrate the spatiotemporal variation of O<sub>3</sub> in China on an annual basis from 1999 to 2017, aiming to explore the response of summer O<sub>3</sub> interannual (1999 to 2017) variation to the WPSH, the period matching the significantly increasing trend of the WPSH-II (Supporting Information (SI), Inset figure of **Fig. S2**), which may lead to a more robust response of the O<sub>3</sub> time series to the WPSH. The results of the first and second EOF patterns for both periods are presented in **Fig. 2**. Each EOF spatial pattern represents a share of the total variation of surface ozone proportional to its eigenvalue. The first EOF loadings (PCA1) are associated strongly with the mean summer O<sub>3</sub> concentrations averaged over the six UAs in China at the correlation coefficient of 0.95 ( $p < 0.01$ ) from 1999 to 2017. The EOF1 pattern also illustrates similarities with the mean summer O<sub>3</sub> concentrations and its standard deviations (**Fig. 1a** and **1b**), featured by large values in central China. Differing from the EOF1, the EOF2 patterns show a south-north contrast pattern. During this period, the first EOF pattern (EOF1) explains 67.4% of the total variance in summer O<sub>3</sub>, and the second EOF pattern (EOF2) explains 9.7% of the total variance. The negative and positive values in the EOF patterns are expected to represent the extent of departures from the average summer ozone. Since the EOF1 pattern is the maximum possible fraction of the variability in the original data, in our case, it explains most of the summer O<sub>3</sub> variability, featured by the growing trends of summer O<sub>3</sub> concentrations. The EOF1 pattern appears to agree, to a large extent, with measured summer (June to August) and warm season (April to September) MDA8 (maximum 8h

277 average) O<sub>3</sub> distribution (Lu et al., 2018; Liu, 2020). The EOF2 patterns also agree with  
 278 the second EOF pattern that Yin et al. (2019) obtained, though their EOF analysis  
 279 focused on daily O<sub>3</sub> in eastern China. The result suggests that the NCP suffered from  
 280 higher O<sub>3</sub> pollution and was also subject to O<sub>3</sub> evolution during the past decades.  
 281



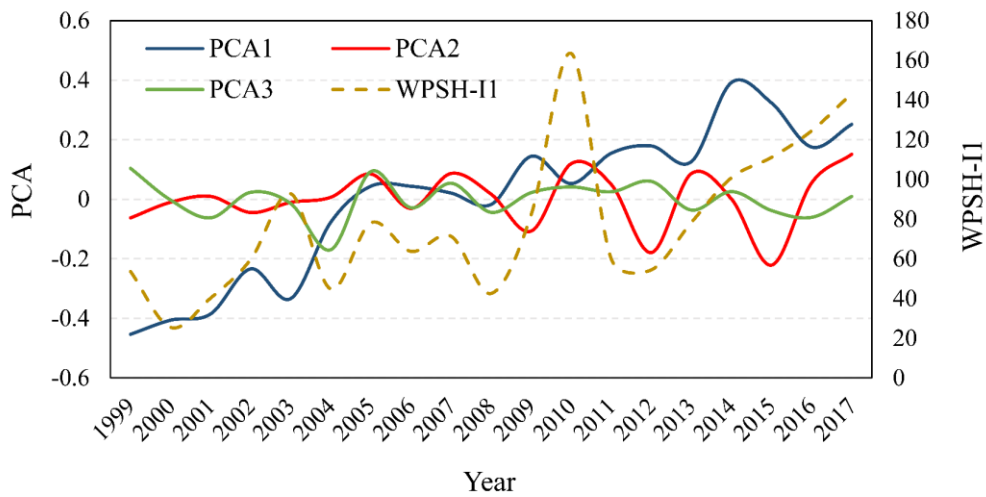
282  
 283 **Figure 2.** First (a) and second (b) EOF patterns across China from 1999 to 2017.

284

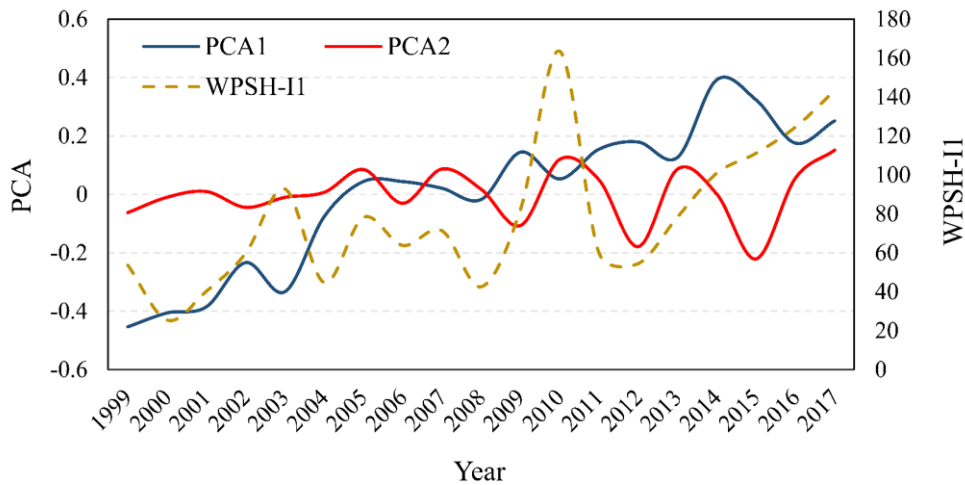
285 The EOF1 shown in **Figs. 2a** suggests that the most significant variations in  
 286 summer O<sub>3</sub> occurred in inland areas of China, extending from Sichuan Province to the  
 287 middle and lower reaches of the Yangtze River and from Hunan to Shanxi Province.  
 288 This inland region covers several major ~~urban agglomerations (UAs)~~ in China,  
 289 including Central China (CC), Middle Reaches of the Yangtze River (MYR), and  
 290 Chengyu (CY, Chengdu–Chongqing) urban agglomeration (Zhang et al., 2022). We  
 291 estimated the correlation coefficients between the first EOF loading (PCA1) and  
 292 summer O<sub>3</sub> concentrations in the six UAs, where 34.3% of China's population resides.  
 293 The results are presented in **Fig. S4**. Strong statistically significant correlations were  
 294 found in CC ( $r = 0.86, p < 0.01$ ), CY ( $r = 0.92, p < 0.01$ ), and MYR ( $r = 0.90, p < 0.01$ ).  
 295 Whereas, in the other three UAs located near the coastal regions, namely the YRD,  
 296 PRD, and BTH, the correlation coefficients range from 0.36 to 0.51 (**Fig. S4**). In  
 297 particular, the PCA1 exhibits more strong association with the summer O<sub>3</sub> anomalies  
 298 averaged over the six UAs, reaching  $r = 0.94$  ( $p < 0.01$ ). The good correlations between  
 299 O<sub>3</sub> concentrations and PCA1 are expected because, as aforementioned in section 3.1  
 300 that, the EOF analysis was carried out by using summer O<sub>3</sub> concentrations as the  
 301 original field that have been increasing during the past decades. However, the

302 magnitude of the correlation coefficients helps identify the extent of O<sub>3</sub> pollution and  
 303 long-term growth trends in China and different UAs (or regions). Overall, these results  
 304 confirm a more substantial interannual variation of summer O<sub>3</sub> in the inland areas than  
 305 in coastal regions of southern and southeastern China.

306



307



308

309 **Figure 3.** Annual variation of ~~three~~ two EOF loadings (PCA1-~~3~~ and 2, scaled on the left Y-axis) and  
 310 WPSH-I1 (dashed brown line, scale on the right Y-axis) from 1999 to 2017.

311

312 **Figure 3** shows annual variations of the ~~three~~ two EOF loadings (PCA1-~~3~~), scaled  
 313 on the left Y-axis) and the WPSH-I1 (dashed brown line, scaled on the right Y-axis)  
 314 from 1999 to 2017. The first EOF loading (PCA1) and WPSH-I1 exhibit growing trends  
 315 during this period with a correlation coefficient of 0.56 ( $p < 0.01$ ). PCA2 shows no clear  
 316 trend and hence is not associated with WPSH-I1. The increasing trend of WPSH-I1

317 since 1999 likely anticipates the interdecadal variation of the WPSH for the recent two  
318 decades. Since O<sub>3</sub> concentrations are positively correlated with the WPSH-I1 (**Figs. 3-**  
319 **5 and 4**), stronger WPSH intensity might elevate summer O<sub>3</sub> levels in China on an  
320 annual basis, particularly the areas with large EOF1 values in inland China (**Fig. 2a**).  
321 However, this conclusion is not well applicable in the PRD region, where we observed  
322 the lowest association between the EOF1 and summer O<sub>3</sub> concentrations (**Fig. 2**) and  
323 between the WPSH-I1 and O<sub>3</sub> levels among the six UAs and over China (**Fig. S4**). It is  
324 also worthwhile to note that, because O<sub>3</sub> precursor emissions in China have been  
325 growing during the past two decades and modeled concentrations were mainly  
326 attributed to precursor emissions, the positive correlations between O<sub>3</sub> concentrations  
327 and the WPSH-I1 should not be understood that the WPSH drove elevated O<sub>3</sub> for a  
328 long term perspective. Further discussions are provided in the next section.

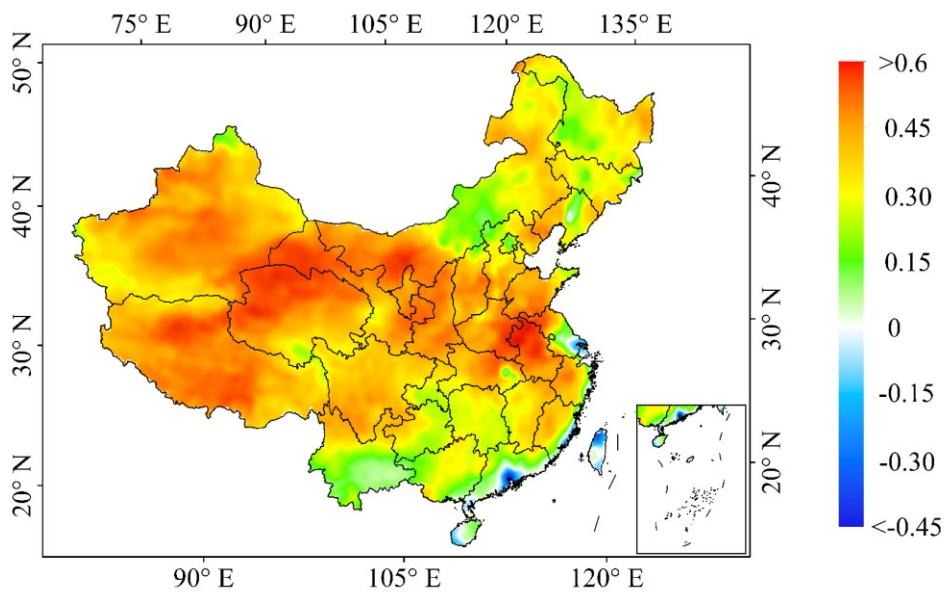
329 We further compared the 500-hPa geopotential heights (GH, gpm) anomalies in  
330 the positive and negative phases of PCA1 and WPSH-I1 as the departure from their  
331 respective means averaged from 1999 to 2017. We selected those years with the  
332 positive and negative anomalies of the PCA1 and WPSH-I1  $\geq \pm 1$  standard deviation  
333 (STD, referred to as the positive and negative phase hereafter) and then estimated their  
334 composite means. The results are shown in **Figs. S5 and S6**. It can be seen that the  
335 composite means of 500-hPa geopotential height in the positive and negative phases of  
336 the PCA1 and WPSH-I1 illustrate good spatial similarities, again demonstrating the  
337 connections between summer O<sub>3</sub> and WPSH-I1. In the positive phase, positive  
338 geopotential height anomalies at the 500-hPa governed China, except for the NCP  
339 regions, including the BTH urban agglomeration, where negative anomalies of the 500-  
340 hPa geopotential heights are observed. On the other hand, a south-north contrast pattern  
341 of the geopotential height composite anomalies is discerned in the negative phase of  
342 the PCA1 and WPSH-I1. The spatial patterns of GH composite anomalies in the  
343 positive and negative phases of the EOF1 also exhibit some similarities with the GH  
344 composite anomalies based on positive and negative O<sub>3</sub> concentration anomalies as the  
345 departure from mean O<sub>3</sub> levels averaged over the six UAs in China from 1999 to 2017  
346 (**Fig. S6**).

### 347 3.2. Associations of summer O<sub>3</sub> with WPSH

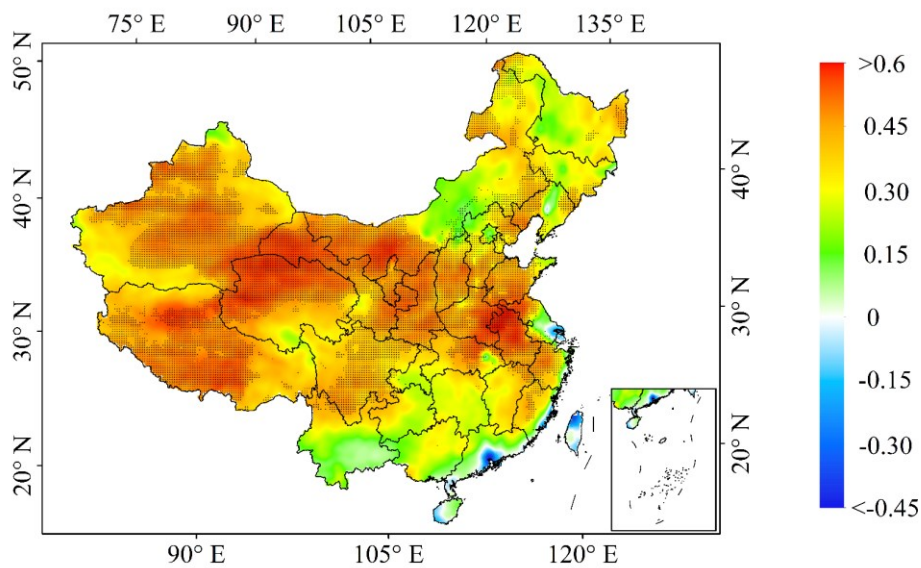
348 Having established the relationships between summer O<sub>3</sub> and WPSH via the EOF  
349 analysis, we further explore the direct responses of summer O<sub>3</sub> to WPSH. Since the  
350 effects of the WPSH span vast regions, and the changes in surface ozone concentrations  
351 may be influenced by the variations in meteorological factors associated with the  
352 WPSH, a spatial correlation analysis between summer surface ozone concentrations in  
353 China and WPSH (WPSH-II) index from 1999 to 2017 was conducted. The result is  
354 illustrated in **Fig. 4**. During this period, positive correlations overwhelm mainland  
355 China, except for the PRD region (**Fig. 4**). ~~Surprisingly, the negative correlations in the~~  
356 ~~PRD region might suggest that the stronger WPSH tends to reduce the summer O<sub>3</sub> in~~  
357 ~~this well-developed and populated UA in China, as aforementioned above. The summer~~  
358 ~~O<sub>3</sub> level in the PRD was the lowest among the six UAs (Figs. 1 and S3). No statistically~~  
359 ~~significant O<sub>3</sub> trend was identified in the PRD, likely attributed to O<sub>3</sub> pollution control~~  
360 ~~in the early 2000s under the joint efforts from Hong Kong and Guangdong provincial~~  
361 ~~governments to improve the air quality in the PRD and Hong Kong (Wu et al., 2013).~~  
362 ~~We also estimated the correlations between O<sub>3</sub> concentrations averaged over the six~~  
363 ~~UAs across China and the WPSH-II from 1999 to 2017 (Fig. S7). The positive~~  
364 ~~correlation coefficients between the mean O<sub>3</sub> concentrations and the WPSH-II in each~~  
365 ~~of the UAs are presented at the top of each column. The results suggest that increasing~~  
366 ~~WPSH-II plays a specific role in elevated O<sub>3</sub> levels in eastern China and these UAs.~~  
367 ~~Again, as aforementioned, a decadal scale increasing WPSH-II trend occurred since~~  
368 ~~the late 1990s and early 2000s (Fig. S1), which seems coincident with the rapidly~~  
369 ~~increasing O<sub>3</sub> precursor emissions and concentration trends in China and its major~~  
370 ~~urban areas (Liu and Wang, 2020; Lu et al., 2018). Hence, the positive correlations~~  
371 ~~between the summer WPSH-II and O<sub>3</sub> concentrations might not be attributable, to a~~  
372 ~~large extent, to growing O<sub>3</sub> pollution. Further discussions are presented in section~~  
373 ~~3.3~~The summer O<sub>3</sub> level in the PRD was the lowest among the six UAs (Figs. 1 and  
374 S3). The causes of the lack of statistically significant O<sub>3</sub> trend and negative correlation  
375 between WPSH-II and O<sub>3</sub> in the PRD might be complex. The stronger WPSH and its

376 westward extension can yield high temperature and dry weather condition in the PRD,  
377 which is conducive to elevated O<sub>3</sub> concentration, and vice versa. Figure S7 shows  
378 relatively strong positive correlation between SAT and WPSH-II, which favors  
379 growing O<sub>3</sub> concentrations, and negative correlation between precipitation and WPSH-  
380 II precipitation, which removes O<sub>3</sub> concentrations from air in the PRD region. From  
381 the early 2000s, Hong Kong and Guangdong provincial governments jointly lunched  
382 an O<sub>3</sub> pollution control program, which significantly reduced O<sub>3</sub> precursor emissions  
383 and its atmospheric levels in the PRD (Wu et al., 2013). It is likely that the course of  
384 O<sub>3</sub> reduction in the PRD coincided with the period of our modeling investigation, which  
385 interferes the statistical correlation between WPSH and O<sub>3</sub> in the PRD.

386



387



388

389 **Figure 4.** Correlation coefficients between summer O<sub>3</sub> concentrations and WPSH-I1 across China  
 390 from 1999 to 2017 on the interdecadal scale: under model scenario 1. The areas filled with black  
 391 dots indicate the regions where the correlation is statistically significant (p<0.05).

392 –

393

394 Considering that summer precipitation in China is sensitive to the western ridge  
 395 point of the WPSH, (Jiang et al., 2021; Yang et al., 2022; Zhao and Wang, 2017), we  
 396 also examined the responses of meteorological fields to the changes in the western ridge  
 397 point index of the WPSH (referred to as the WPSH-I2) subject to its positive and  
 398 negative phases. The WPSH-I2 is opposite to the WPSH-I1 (**Fig. S8**). We estimated  
 399 WPSH-I2 anomalies as the departure from its mean from 1999 to 2017. We defined the  
 400 positive WPSH-I2 phase if its values are greater than one standard deviation and the  
 401 negative phase if WPSH-I2 < one standard deviation. The annual summer mean  
 402 meteorological variables in the positive and negative phases of the WPSH-I2 are  
 403 summed to obtain their respective composite means. We then calculated the anomalies  
 404 of these composite means by subtracting their respective long-term means averaged  
 405 from 1990 to 2022. **Figure 5** shows the anomalies of composite means of 500-hPa GH,  
 406 precipitation (cm/mn), and the surface air temperature (SAT, °C) across China in the  
 407 positive and negative phases of WPSH-I2. The results identified evident north-south  
 408 contrast for all three meteorological variables in the positive phase of the WPSH-I2. Of



409 which, the anomalies of GH composite means are positive in northern China with a  
410 center in Mongolia and northeastern China (**Fig. 5a**). In contrast, the broad region to  
411 the south of 35°N is under the regime of negative GH composite anomalies (**Fig. 5b**).  
412 The 500-hPa GH patterns can also be confirmed by the anomalies of composite mean  
413 sea level pressure (SLP) in the positive and negative phase of WPSH-I2 (**Fig. 6**),  
414 showing negative SLP anomalies from the Bay of Bengal to the tropical western Pacific  
415 in the positive phase of the WPSH-I2 and positive anomalies covering a vast region  
416 from southeast to northeast China. The south-north dipole patterns of 500-hPa GH  
417 composite anomalies in **Fig. 5a** and the SLP composite anomalies in **Fig. 6** often  
418 accompany the termination of the rain season in southern China and the start of the  
419 rainy season in northern China (Nie et al., 2021), as shown by the negative rainfall  
420 anomaly in southern China and positive anomaly in northern China. **Figure 5a** predicts  
421 the weakening WPSH or the northward movement of the WPSH, leading to a southward  
422 pressure gradient, as shown in **Fig. 5a**. As a result, the composite anomalies of 850-hPa  
423 vector winds illustrate northerly wind components over central-south and southern  
424 China (**Fig. 6**). Such northerly wind anomalies do not favor southward water vapor  
425 transport by southwesterly Indian monsoon.

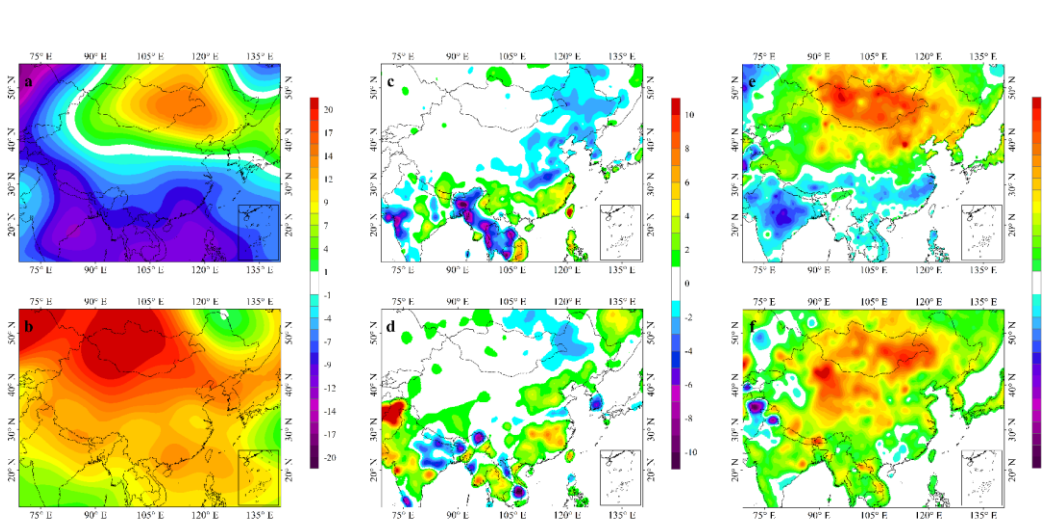
426 On the other hand, easterly and southeasterly wind components extend from  
427 tropical west Pacific to central and northern China, paving a water vapor transport  
428 pathway and corresponding to the positive rainfall anomaly in this part of China (**Fig.**  
429 **5c**). In the negative phase of the WPSH-I2, positive SLP anomalies overwhelmed  
430 eastern China with a center in the coastal region of southern China, implying the  
431 enhancement of the WPSH. Accordingly, we observe negative composite anomalies of  
432 the precipitation extending from the Yangtze-Huaihe Valley from central to  
433 northeastern China, suggesting declining precipitations in these regions. Growing  
434 precipitations are seen in southern and southeastern China, characterized by the positive  
435 composite anomalies of the precipitation (**Fig. 5c**).

436 Precipitations in China have been connected strongly with the WPSH-I2 from a  
437 daily perspective (Duan et al., 2008; Nie et al., 2021). Along with the westward shifting  
438 of the WPSH ridge point, the major rain belt moves northward to the middle and lower

439 reaches of the Yangtze River from June to mid-July and northern and northeastern  
440 China from late July to mid-August (Lu et al., 2017; Su et al., 2014; Zhao and Wang,  
441 2017). In our case, with the focus on the association between summer O<sub>3</sub> and WPSH  
442 from the interannual perspective, we show that the growing summer rainfall in southern  
443 and southeastern China is associated with stronger WPSH in an east position, featured  
444 by negative GH composite anomalies to the south of 35°N in China (**Fig. 5a**). Such GH  
445 anomaly pattern does not favor atmospheric water vapor transport to North China by  
446 the summer monsoon circulations (Nie et al., 2021), which results in low rainfall in this  
447 part of China (**Fig. 5c**). Accordingly, relatively higher SATs are observed in North  
448 China (**Fig. 5e**), which, together with low atmospheric humidity and rainfall, favors O<sub>3</sub>  
449 formation and evolution. On the other hand, the stronger rainfall in southern and  
450 southeastern China caused lower SATs in this region, characterized by negative SAT  
451 composite anomalies (**Fig. 5e**). The higher atmospheric humidity, stronger rainfall or  
452 precipitation washout, and lower SATs tend to restrain O<sub>3</sub> formation in southern China,  
453 which resulted in lower O<sub>3</sub> levels compared to that measured in central and northern  
454 China (Lu et al., 2018; Liu, 2020). This is likely a reason for higher O<sub>3</sub> concentrations  
455 observed in northern and central-north China, such as the BTH and central China urban  
456 agglomerations, than in YRD and PRD regions. In the negative phase of the WPSH-I2,  
457 the north-south contrast pattern of all three meteorological variables vanished. Instead,  
458 positive GH composite anomalies at the 500-hPa are seen in China, with more muscular  
459 positive anomalies in western Mongolia (**Fig. 5b**). Such GH pattern suggests the  
460 reinforcement and western shift of the WPSH. As a result, the composite anomalies of  
461 the summer precipitation in northern China turned to positive, meaning high rainfall in  
462 this region (**Fig. 5d**). However, the composite anomalies of SATs in the negative phase  
463 of the WPSH-I2 (**Fig. 5f**) seem not to respond well to the intense rainfall, except in the  
464 PRD, where declining SATs, featured by the negative SAT composite anomalies (**Fig.**  
465 **5f**), corresponding well to the positive composite precipitation anomalies, meaning high  
466 rainfall in this region (**Fig. 5d**). This result also is in line with previous observations  
467 that the westward shift of the WPSH ridge point often accompanied with the

468 termination of the systematic rainfall in southern China (Duan et al., 2008; Huang et  
 469 al., 2018; Nie et al., 2021).

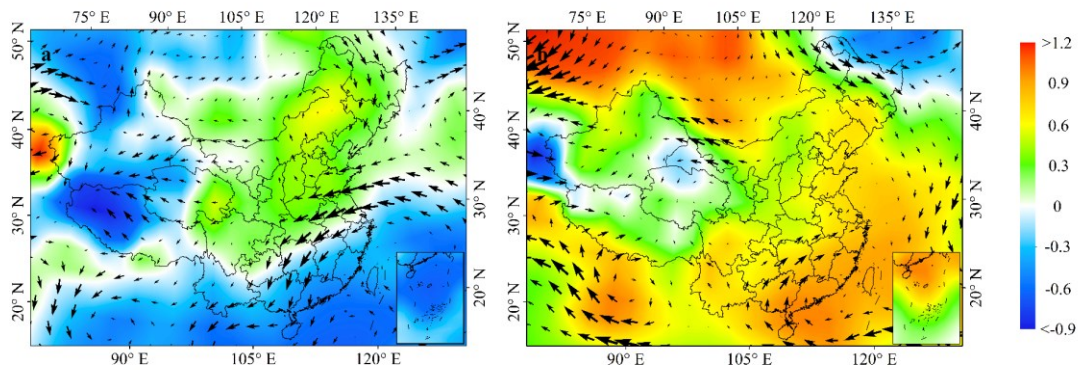
470



471

472 **Figure 5.** Anomalies of composite means of 500-hPa GH (GPH) in positive (a) and negative (b)  
 473 phase of WPSH-I2 from 1999 to 2017; same as Fig. 5a and 5b but for precipitation (cm/mm) in  
 474 positive (c) and negative (d) WPSH-I2 phase; same as Fig. 5a and 5b but for SAT (°C) in positive  
 475 (e) and negative (f) phase of WPSH-I2 from 1999 to 2017.

476



477

478 **Figure 6.** Anomalies of composite means of sea level pressure (SLP, hPa) overlapped with the  
 479 anomalies of composite mean 850-hPa vector winds across China in the positive (a) and negative  
 480 (b) phases of WPSH-I2 from 1999 to 2017.

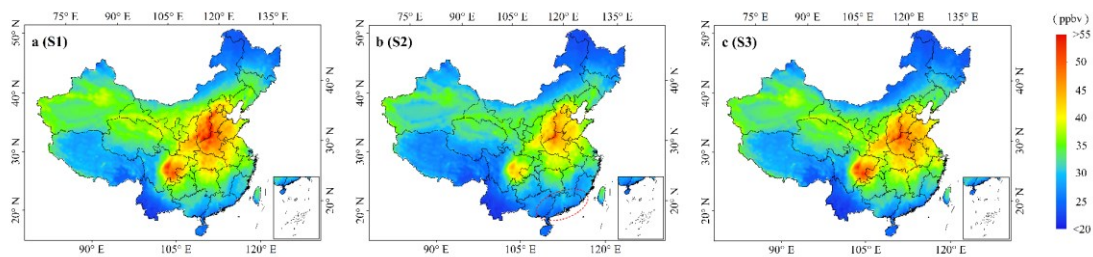
481

### 482 3.3. WPSH and interannual O<sub>3</sub> fluctuations

483 Having identified the associations between the WPSH and O<sub>3</sub> evolution on  
 484 interannual scales, it is also interesting to know to what extent the WPSH could  
 485 contribute to the interannual fluctuations in O<sub>3</sub> concentrations in China and its major

486 ~~urban agglomerations.UAs~~. We compared modeled O<sub>3</sub> concentrations among three  
 487 model scenarios by estimating their differences (fractions). **Figure 7** illustrates summer  
 488 mean O<sub>3</sub> concentrations averaged from 1999 to 2017 from the three scenarios. Identical  
 489 concentration spatial patterns can be observed in scenarios 1 (base, **Fig. 7a**) and 3 (fixed  
 490 meteorology, **Fig. 7c**), suggesting that precursor emissions overwhelmed the spatial-  
 491 temporal distribution of summer ozone in China. Comparing **Figs. 7b** with **Fig. 7a** and  
 492 **7c**, we also notice that the low summer ozone levels simulated from model scenario 2  
 493 (fixed precursor emissions, **Fig. 7b**) extend a much larger area across southern China  
 494 (highlighted by a solid red circle). Considering that model scenarios 1 and 2 used the  
 495 same meteorological data from 1998 to 2017, the lower O<sub>3</sub> levels under scenario 2 can  
 496 be attributed mainly to declining precursor emissions, partly attributable to a  
 497 collaborative effort to mitigate air pollution in the PRD and Hong Kong since the early  
 498 2000s as aforementioned before, which effectively slowed down growing O<sub>3</sub> precursor  
 499 emissions (Wu et al., 2013).

500



501

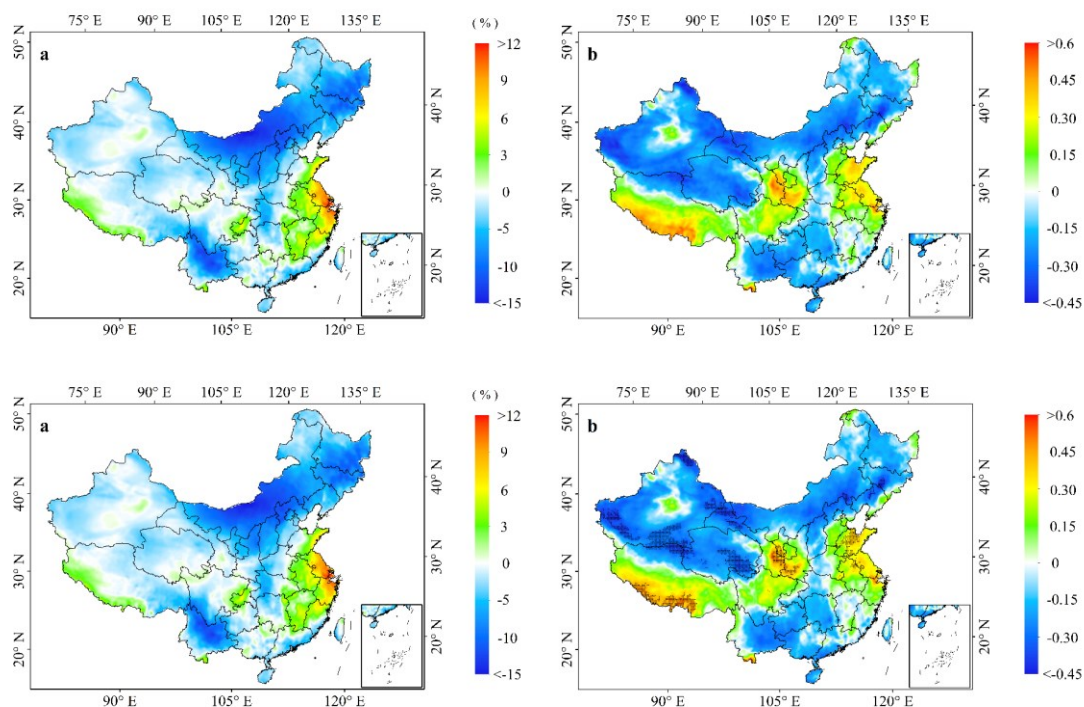
502 **Figure 7.** Modeled mean summer O<sub>3</sub> concentrations across China averaged from 1999 to 2017: (a)  
 503 Model scenario 1 (base scenario), (b) model scenario 2 (fixed precursor emission), and (c) model  
 504 scenario 3 (fixed meteorology).

505

506 To extract signals of meteorology in modeled O<sub>3</sub> concentrations, we calculated the  
 507 percentage change in summer O<sub>3</sub> concentrations subject to model scenarios 1 and 3,  
 508 defined as  $O_{3,frac} = (O_{3(S3)} - O_{3(S1)}) / O_{3(S1)} \times 100\%$ , where  $O_{3(S3)}$  and  $O_{3(S1)}$  represent the  
 509 summer ozone concentrations for scenarios 3 and 1 between 1999 and 2017 (**Fig. 8a**).  
 510 Since both model scenarios 1 and 3 used the same precursor emissions, their differences  
 511 (fractions) can quantify the meteorological effect on O<sub>3</sub> fluctuations. Significantly, the  
 512 WPSH was at a relatively high value in 1998 compared to 1999-2017 (**Fig. S2**). The

513 result shows that the fixed meteorological conditions (scenario 3) resulted in higher  
514 summer ozone concentrations in the eastern seaboard region of China than the results  
515 from the base scenario, particularly in the YRD, where the fixed meteorological  
516 conditions enhanced the summer concentration by >9% compared to the base scenario  
517 modeling result (**Fig. 8a**). The second-highest O<sub>3</sub> fraction between the scenarios 1 and  
518 3 occurred in the Sichuan Basin, where the scenario 3 predicted the summer  
519 concentrations are 3% to 6% higher than the base scenario 1. **Figure 8b** presents the  
520 correlation coefficients between the WPSH-II and scenario 2 modeled O<sub>3</sub>  
521 concentrations across China from 1999 to 2017, showing relatively high positive  
522 correlation coefficients in the eastern seaboard area and the region extending from the  
523 Sichuan Basin to the Gansu-Shaanxi border, like the fractional changes shown in **Fig.**  
524 **8a**. However, the negative correlations extended in most parts of China, indicating that  
525 the WPSH tends to reduce summer O<sub>3</sub> levels in these regions. This spatial correlation  
526 pattern differs significantly from the correlation pattern shown in **Fig. 4**, in which  
527 positive correlations between the summer WPSH and modeled O<sub>3</sub> under the base  
528 scenario almost extend entire China. As aforementioned, this is because both WPSH-  
529 II and O<sub>3</sub> precursor emissions in China increased from 1999 to 2017. **Figure 8** shows  
530 some similarities between spatial distribution patterns of the fractional changes in  
531 summer O<sub>3</sub> concentrations under scenarios 1 and 3 and the correlations of summer O<sub>3</sub>  
532 concentrations from model scenario 2 and the WPSHI-II. The result suggests that the  
533 meteorological conditions contributing to summer O<sub>3</sub> evolution, as shown in **Fig. 8a**,  
534 are associated, to a large extent, with the WPSH. The positive contribution of  
535 meteorology characterized by the positive correlations to elevated O<sub>3</sub> pollution  
536 gradually weakens in inland areas and turns into a negative contribution, meaning the  
537 reduction of summer O<sub>3</sub> by meteorology in inland China, including most northern and  
538 northeastern regions. Although positive correlations were estimated in the Tibet Plateau,  
539 given very low O<sub>3</sub> pollution, the WPSH would not exert any significant influence on  
540 O<sub>3</sub> levels in the plateau. It is worth noting that **Figure 4** shows a negative correlation  
541 between modeled summer O<sub>3</sub> concentration from model scenario 1 and WPSH-I2 time  
542 series in the YRD but model scenario 2 yields a positive correlation (**Fig. 8b**). Since

543 model scenario 1 took annually-altered O<sub>3</sub> precursor emissions into consideration, the  
 544 negative correlation suggests that declining precursor emissions from 1999 to 2017 in  
 545 the YRD overwhelmed the WPSH effect. After removed the effect of precursor  
 546 emissions, the meteorological conditions associated with the WPSH would help  
 547 enhance O<sub>3</sub> concentrations in this region.



550  
 551 **Figure 8.** Fractional changes between modeled O<sub>3</sub> concentrations subject to model scenarios 3 and  
 552 1 from 1999 to 2017 estimated by  $O_{3,frac} = (O_{3(S3)} - O_{3(S1)}) / O_{3(S1)} \times 100\%$  (a), and correlation  
 553 coefficients between summer WPSH-I1 and modeled summer O<sub>3</sub> concentrations under model  
 554 scenario 2 (b). The areas filled with black dots in Fig. 8b indicate the regions where the correlation  
 555 is statistically significant (p < 0.05).

556  
 557 As shown in **Fig. 5c**, the positive WPSH-I1 corresponds to lower precipitation in  
 558 southern and southeastern China and higher precipitation in central and northern China,  
 559 which tends to enhance O<sub>3</sub> levels in southern and southeastern China and reduce O<sub>3</sub>  
 560 concentrations in the north. Although we also observe higher SATs across northern  
 561 China and lower SATs in the south, which should increase O<sub>3</sub> levels in the north and  
 562 decrease O<sub>3</sub> levels in the south, we could not quantify the direct linkages between SATs  
 563 and O<sub>3</sub> concentrations from a national perspective. **Figure S9S7** displays the correlation

564 coefficients between summer WPSH-II and the SAT (**Fig. S9a**S7a) and precipitation  
565 (**Fig. S9b**)-S7b) from 1999 to 2017 across China. We can observe stronger positive  
566 correlations between the WPSH-II and SAT in southern China, indicating that the  
567 WPSH tends to enhance SAT in this region. This should favor elevated O<sub>3</sub>  
568 concentrations instead of the reduction of O<sub>3</sub> levels, as shown in **Fig. 7b**. This result  
569 likely anticipates that stronger precipitation associated with WPSH in this part of China  
570 overwhelmed SAT and overall yielded lower O<sub>3</sub> concentrations in southern China.  
571 Considering strong association of O<sub>3</sub> formation and solar radiation (sunlight), we also  
572 estimated the correlation coefficients between surface incoming solar radiation flux (W  
573 m<sup>-2</sup>) and O<sub>3</sub> concentration and WPSH-II from 1999 to 2017 across China. The results  
574 are illustrated in Fig. S9. The spatial pattern of the correlation coefficients between the  
575 radiation flux and O<sub>3</sub> concentration is similar to the correlation between SAT and  
576 WPSH-II with higher correlations across the China's eastern and southern seaboard  
577 regions (Fig. S9a), implying that O<sub>3</sub> should be more readily formed in these regions,  
578 though O<sub>3</sub> levels were not higher in these regions than Central China and the BTH (Fig.  
579 1), as discussed below. However, no statistically significant positive correlations  
580 between radiation flux and WPSH-II were identified (Fig. S9b)

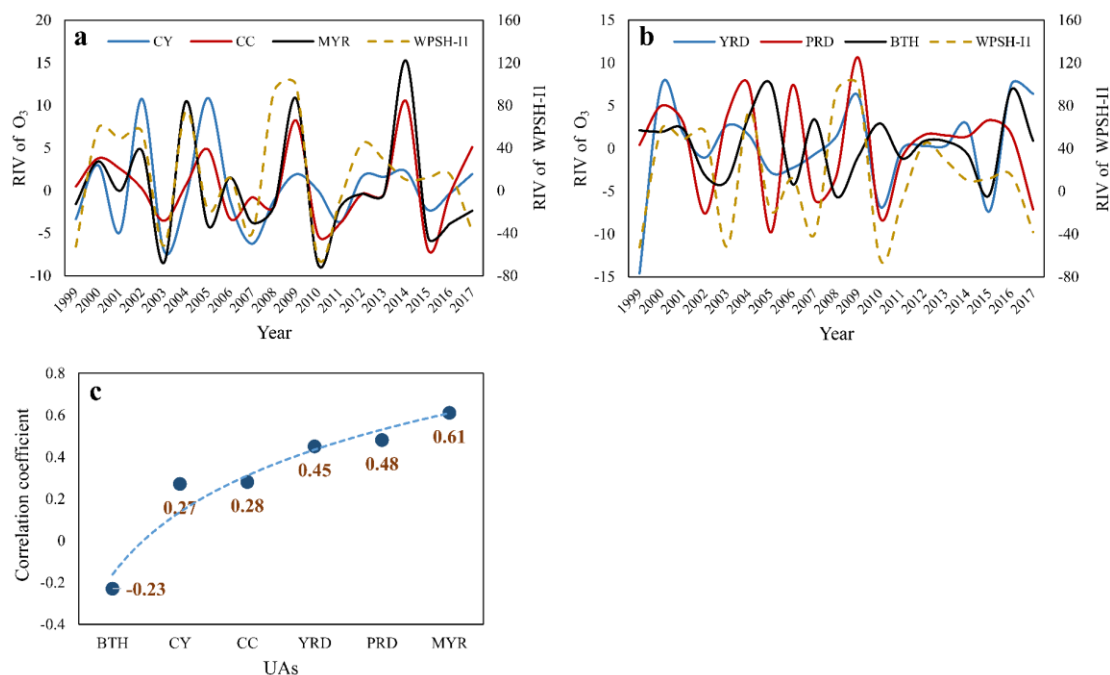
581 **Figure S10** illustrates annual variations of summer averaged O<sub>3</sub> concentrations  
582 under the three model scenarios from 1998 to 2017 over six UAs. Distinct differences  
583 between the three inland UAs (CY, CC, and MYR) and the three coastal UAs (YRD,  
584 PRD, and BTH) can be discerned from more significant fractions with an increasing  
585 trend in CY, CC, and MYR, as compared to YRD, PRD, and BTH, in which there were  
586 no significant trends in modeled concentrations. In the three inland UAs (CY, CC, and  
587 MYR, **Fig. S10d-f**), O<sub>3</sub> concentrations under fixed precursor emissions (scenario 2,  
588 solid red line) are lower markedly than that from scenario 1 (solid green line) and exhibit  
589 no statistically significant temporal trend, suggesting that the variable meteorology  
590 does not contribute significantly to O<sub>3</sub> levels and its long-term temporal trends. On the  
591 other hand, O<sub>3</sub> concentrations under scenarios 1 and 3 runs are more or less similar and  
592 illustrate increasing trends, indicating that growing precursor emissions in the past two  
593 decades dominate long-term O<sub>3</sub> evolution in these inland UAs. In the three coastal UAs

594 (PRD, YRD, and BTH), the increasing trends of modeled summer O<sub>3</sub> under scenario 3  
595 were less significant than in the three inland UAs, indicating slower growth of precursor  
596 emissions in these coastal UAs. No significant increasing trends of O<sub>3</sub> concentrations  
597 from scenario 3 run (fixed emission in 1998) are observed, suggesting that the changes  
598 in meteorological conditions in the past two decades contributed less to growing O<sub>3</sub>  
599 pollution in China's major urban clusters than precursor emissions. However, we  
600 noticed from **Fig. S10** that annual fluctuations of summer O<sub>3</sub> concentrations in these  
601 UAs under scenario 2 agree, to a large extent, with the results from model scenario 1  
602 (base scenario). This is expected because the two model scenarios shared the same  
603 meteorology. As a result, precursor emissions contributed primarily to the long-term  
604 O<sub>3</sub> growing trends and magnitudes, whereas meteorology made more vital  
605 contributions to interannual fluctuations of O<sub>3</sub> concentrations.

606 To link the interannual fluctuations of summer ozone induced by meteorology  
607 with WPSH, we estimated the rate of interannual variation (RIV) of summer O<sub>3</sub>  
608 concentrations simulated by model scenario 2 in the 6 UAs and WPSH-II, given by  $C_r$   
609 =  $[c(n) - c(n-1)]/c(n-1) \times 100\%$ , where  $c(n)$  and  $c(n-1)$  are summer O<sub>3</sub> concentrations in  
610 the current year and previous year, respectively. The same approach also calculated the  
611 RIV of summer WPSH-II. **Figures 9a** and **9b** present the RIV of summer O<sub>3</sub>  
612 concentrations in the three inland and coastal UAs, respectively. The RIV of the WPSH-  
613 II is also shown in the figure (brown dashed line). Although these RIVs do not exhibit  
614 significant trends, we can observe a general agreement of the RIV between the  
615 WPSH-II and summer O<sub>3</sub> concentrations in most UAs, featured by their annual  
616 oscillations. **Figure 9c** shows the correlation coefficients between the RIVs of the  
617 summer WPSH-II and O<sub>3</sub> concentrations. The highest correlation is found in the MYR,  
618 followed by the PRD and YRD, whereas the lowest correlation occurred in the BTH.  
619 These correlations suggest that the O<sub>3</sub> interannual fluctuations in those areas proximate  
620 to the WPSH tend to be more strongly associated with the WPSH, regardless of the  
621 positive or negative effect of the WPSH on O<sub>3</sub> evolution. This is because, as a large-  
622 scale high-pressure system, the WPSH affects significantly on its surrounding weather  
623 conditions, which, in turn, perturbs O<sub>3</sub> concentrations in its nearby regions. Since the



624 meteorology determined largely the interannual fluctuations of summer O<sub>3</sub> and  
 625 connected nicely with the WPSH, the associations of the RIVs between summer the  
 626 WPSH-II and O<sub>3</sub> concentrations imply that the WPSH made a more stronger  
 627 contribution to the interannual variation of summer O<sub>3</sub>, rather than its long-term trend,  
 628 though the WPSH-II presents an increasing trend after 1998 (**Fig. 3**).  
 629



630  
 631 **Figure 9.** (a) Rate of interannual variations of summer WPSH-II (brown dashed line) and O<sub>3</sub> in CY,  
 632 CC, and MYR from 1999 to 2017, (b) same as Fig. 9a but for YRD, PRD, and BTH, and (c)  
 633 correlation coefficients of the rate of interannual variations of summer WPSH-II and O<sub>3</sub> in six UAs  
 634 from 1999 to 2017.

635

#### 636 4. Conclusions

637 Model simulations revealed higher O<sub>3</sub> concentrations from 1999 to 2017 in the  
 638 Sichuan Basin and the region extending from central China to the NCP, agreeing with  
 639 measured mean summer concentrations. The first EOF loadings (PCA1) are associated  
 640 strongly with the mean summer O<sub>3</sub> concentrations across China and its major UAs- with  
 641 the correlation coefficient  $r=0.56$  ( $P \leq 0.01$ ). We identified distinctive differences  
 642 between positive and negative WPSH anomalies and elucidated their impacts on  
 643 interannual variation of O<sub>3</sub> and meteorological conditions. In some of the UAs, such as

644 the PRD, where relatively lower O<sub>3</sub> levels were reported compared to other major UAs;  
645 ~~the WPSH tended to reduce O<sub>3</sub> levels.~~ The EOF and regression analysis revealed  
646 stronger responses of summer O<sub>3</sub> simulated under model scenario 2 (fixed precursor  
647 emission) in the region extending from southeastern to central China with the highest  
648 correlation of 0.7 in the MYR. We noted that WPSH became stronger since the late  
649 1990s and early 2000s, featured by the enhancing WPSH index after 1999. As a result,  
650 stronger associations between summer O<sub>3</sub> in China and its primary UAs and the WPSH  
651 occurred in the recent two decades. Extensive model scenario simulations indicated that  
652 precursor emissions dominated the long-term trend and magnitude of summer ozone  
653 concentrations. However, the meteorology associated with the WPSH largely  
654 determined their interannual fluctuations from 1999 to 2017, demonstrated by the  
655 positive correlation coefficients between RIV and WPSH-II in China's major UAs  
656 (except for BTH), ranging from 0.27 to 0.61. Our results concluded that the influence  
657 of precursor emissions on the evolution of ozone was stronger in Chengdu-Chongqing,  
658 the middle reaches of the Yangtze River, and central China than in the coastal city  
659 clusters. However, the influence of meteorological conditions is not significant. In  
660 contrast, for the coastal city clusters of the Yangtze River Delta, the Pearl River Delta,  
661 and the Beijing-Tianjin-Hebei region, the influence of precursor emissions on the  
662 summer ozone evolution is weaker than in the inland city clusters, but the influence of  
663 meteorological conditions was greater than in the inland city clusters, particularly in  
664 those urban areas proximate to the WPSH. Considering the great efforts in China to  
665 mitigate O<sub>3</sub> pollution via reducing anthropogenic precursor emissions, interannual and  
666 longer-term O<sub>3</sub> evolutions associated with increasing WPSH strength might be worth  
667 paying attention because it might influence background O<sub>3</sub> concentration, its long-term  
668 prediction, and long-term O<sub>3</sub> mitigation measures. The results from the present study  
669 might also imply that the local policy makers in different UAs should take the WPSH's  
670 impacts into account in making their respective O<sub>3</sub> reduction strategies, in addition to  
671 precursor emissions. To the end, it is worth noting that this modeling study was partly  
672 based on an increasing trend of the summer WPSH strength since 2000, which  
673 coincided with growing O<sub>3</sub> evolution. Historically, the WPSH has been fluctuated on a

674 yearly basis. Further study needs to be conducted to discern the associations between  
675 projected WPSH and O<sub>3</sub> concentrations subject to future climate change scenarios, such  
676 as shared socioeconomic pathways under Coupled Model Intercomparison Project  
677 (CMIP6) and the Intergovernmental Panel on Climate Change (O'Neill et al., 2017).

678

679

#### 680 **Code/Data availability**

681 Data will be made available on request.

682

#### 683 **Author contributions**

684 All authors contributed to the manuscript and have given approval of the final version.  
685 XZ, RZ and XJ designed the research. XZ, XL and KC collected the data. ST, JL, HG  
686 and TH contributed to the interpretation of results. XZ, RZ and JM wrote and revised  
687 the manuscript.

688

#### 689 **Competing interests**

690 The authors declare that they have no known competing financial interests or personal  
691 relationships that could have appeared to influence the work reported in this paper.

692

#### 693 **Financial support**

694 This study is supported by the National Natural Science Foundation of China  
695 (41991312, 41977357).

696

#### 697 **Appendix A. Supplementary data**

698 Supplementary data to this article can be found online

699

#### 700 **References**

701 Akimoto, H., Mori, Y., Sasaki, K., Nakanishi, H., Ohizumi, T., and Itano, Y.: Analysis of monitoring  
702 data of ground-level ozone in Japan for long-term trend during 1990–2010: Causes of temporal  
703 and spatial variation, *Atmos. Environ.*, 102, 302–310,  
704 <https://doi.org/10.1016/J.ATMOENV.2014.12.001>, 2015.

705 Bell, M. L., Zanobetti, A., and Dominici, F.: Who is more affected by ozone pollution? A systematic  
706 review and meta-analysis, *American Journal of Epidemiology*, 180, 15–28,  
707 <https://doi.org/10.1093/aje/kwu115>, 2014.

708 Brauer, M., Amann, M., Burnett, R. T., Cohen, A., Dentener, F., Ezzati, M., Henderson, S. B.,  
709 Krzyzanowski, M., Martin, R., van Dingenen, R., van Donkelaar, A., and Thurston, G. D.:  
710 Exposure assessment for estimation of the global burden of disease attributable to outdoor air  
711 pollution, *Environ. Sci. Technol.*, 46, 652–660, <https://doi.org/10.1021/es2025752>, 2012.

- 712 Chen, Z., Li, R., Chen, D., Zhuang, Y., Gao, B., Yang, L., and Li, M.: Understanding the causal  
713 influence of major meteorological factors on ground ozone concentrations across China, *J.*  
714 *Clean. Prod.*, 242, 118498, <https://doi.org/10.1016/j.jclepro.2019.118498>, 2020.
- 715 Dang, R., Liao, H., and Fu, Y.: Quantifying the anthropogenic and meteorological influences on  
716 summertime surface ozone in China over 2012–2017, *Sci. Total Environ.*, 754, 142394,  
717 <https://doi.org/10.1016/j.scitotenv.2020.142394>, 2021.
- 718 Ding, D., Xing, J., Wang, S., Chang, X., and Hao, J.: Impacts of emissions and meteorological  
719 changes on China’s ozone pollution in the warm seasons of 2013 and 2017, *Front. Environ.*  
720 *Sci. Eng.*, 13, 76, <https://doi.org/10.1007/s11783-019-1160-1>, 2019.
- 721 Duan, L., Rong, Y., and Liang, P.: Effect of West Pacific Subtropical High on Summer Precipitation  
722 in North China, *Met. Sci. Technol.*, 36, 273–276, [http://www.cnki.com.cn/Article/CJFDTotal-](http://www.cnki.com.cn/Article/CJFDTotal-QXKJ200803004.htm)  
723 [QXKJ200803004.htm](http://www.cnki.com.cn/Article/CJFDTotal-QXKJ200803004.htm), 2008.
- 724 Fiore, A. M., Jacob, D. J., Mathur, R., and Martin, R. V.: Application of empirical orthogonal  
725 functions to evaluate ozone simulations with regional and global models, *J. Geophys. Res.*  
726 *Atmos.*, 108, <https://doi.org/10.1029/2002jd003151>, 2003.
- 727 Fleming, Z. L., Doherty, R. M., von Schneidmesser, E., Malley, C. S., Cooper, O. R., Pinto, J. P.,  
728 Colette, A., Xu, X., Simpson, D., Schultz, M. G., Lefohn, A. S., Hamad, S., Moolla, R., Solberg,  
729 S., and Feng, Z.: Tropospheric Ozone Assessment Report: Present-day ozone distribution and  
730 trends relevant to human health, *Elementa*, 6, 12, <https://doi.org/10.1525/elementa.273>, 2018.
- 731 Fu, Y., Liao, H., and Yang, Y.: Interannual and Decadal Changes in Tropospheric Ozone in China  
732 and the Associated Chemistry-Climate Interactions: A Review, *Adv. Atmos. Sci.*, 36, 975–993,  
733 <https://doi.org/10.1007/s00376-019>, 2019.
- 734 Guenther, A. B., Jiang, X., Heald, C. L., Sakulyanontvittaya, T., Duhl, T., Emmons, L. K., and Wang,  
735 X.: The Model of Emissions of Gases and Aerosols from Nature version 2.1 (MEGAN2.1): an  
736 extended and updated framework for modeling biogenic emissions, *Geosci. Model Dev.*, 5,  
737 1471–1492, <https://doi.org/10.5194/gmd-5-1471-2012>, 2012.
- 738 Han, H., Liu, J., Shu, L., Wang, T., and Yuan, H.: Local and synoptic meteorological influences on  
739 daily variability in summertime surface ozone in eastern China, *Atmos. Chem. Phys.*, 20, 203–  
740 222, <https://doi.org/10.5194/acp-20-203-2020>, 2020.
- 741 Huang, Y., Wang, B., Li, X., and Wang, H.: Changes in the influence of the western Pacific  
742 subtropical high on Asian summer monsoon rainfall in the late 1990s, *Clim. Dyn.*, 51, 443–  
743 455, <https://doi.org/10.1007/s00382-017-3933-1>, 2018.
- 744 Jiang, Z., Li, J., Lu, X., Gong, C., Zhang, L., and Liao, H.: Impact of western Pacific subtropical  
745 high on ozone pollution over eastern China, *Atmos. Chem. Phys.*, 21, 2601–2613,  
746 <https://doi.org/10.5194/acp-21-2601-2021>, 2021.
- 747 Lefohn, A. S., Malley, C. S., Simon, H., Wells, B., Xu, X., Zhang, L., and Wang, T.: Responses of  
748 human health and vegetation exposure metrics to changes in ozone concentration distributions  
749 in the European Union, United States, and China, *Atmos. Environ.*, 152, 123–145,  
750 <https://doi.org/10.1016/j.atmosenv.2016.12.025>, 2017.
- 751 Li, K., Jacob, D. J., Liao, H., Shen, L., Zhang, Q., and Bates, K. H.: Anthropogenic drivers of 2013–

752 2017 trends in summer surface ozone in China, *Proc. Natl. Acad. Sci. U. S. A.*, 116, 422–427,  
753 <https://doi.org/10.1073/pnas.1812168116>, 2019.

754 Li, K., Jacob, D.J., Shen, L., Lu, X., de Smedt, I., and Liao, H.: Increases in surface ozone pollution  
755 in China from 2013 to 2019: Anthropogenic and meteorological influences, *Atmos. Chem.  
756 Phys.*, 20, 11423–11433, <https://doi.org/10.5194/acp-20-11423-2020>, 2020.

757 Lin, C. Q., Lau, A. K. H., Fung, J. C. H., Song, Y. S., Li, Y., Tao, M. H., Lu, X. C., Ma, J., and Lao,  
758 X. Q.: Removing the effects of meteorological factors on changes in nitrogen dioxide and  
759 ozone concentrations in China from 2013 to 2020, *Sci. Total Environ.*, 793, 148575,  
760 <https://doi.org/10.1016/j.scitotenv.2021.148575>, 2021.

761 Lin, Y., Zhang, L., Fan, Q., Meng, H., Gao, Y., Gao, H., and Yao, X.: Decoupling impacts of weather  
762 conditions on interannual variations in concentrations of criteria air pollutants in South China  
763 – constraining analysis uncertainties by using multiple analysis tools, *Atmos. Chem. Phys.*, 22,  
764 16073–16090, <https://doi.org/10.5194/acp-22-16073-2022>, 2022.

765 Liu, H., Liu, S., Xue, B., Lv, Z., Meng, Z., Yang, X., Xue, T., Yu, Q., and He, K.: Ground-level  
766 ozone pollution and its health impacts in China, *Atmos. Environ.*, 173, 223–230,  
767 <https://doi.org/10.1016/j.atmosenv.2017.11.014>, 2018.

768 Liu, J.: Ozone regionalization and evolution characteristics, and meteorological formation  
769 mechanism in China from 2013 to 2018, Ph.D. thesis, [http://cdmd.cnki.com.cn/article/cdmd-  
770 10300-1021778486.htm](http://cdmd.cnki.com.cn/article/cdmd-10300-1021778486.htm), 2020.

771 Liu, Q., Zhou, T., Mao, H., and Fu, C.: Decadal variations in the relationship between the western  
772 Pacific subtropical high and summer heat waves in east China, *J. Clim.*, 32, 1627–1640,  
773 <https://doi.org/10.1175/JCLI-D-18-0093.1>, 2019a.

774 Liu, Y., Liang, P., and Sun, Y.: Characteristics of the Western Pacific Subtropical High and Summer  
775 Rainfall Anomalies, *The Asian Summer Monsoon*, 85–95, [https://doi.org/10.1016/B978-0-12-  
776 815881-4.00005-6](https://doi.org/10.1016/B978-0-12-815881-4.00005-6), 2019b.

777 Liu, Y., and Wang, T.: Worsening urban ozone pollution in China from 2013 to 2017 - Part 1: The  
778 complex and varying roles of meteorology, *Atmos. Chem. Phys.*, 20, 6305–6321,  
779 <https://doi.org/10.5194/acp-20-6305-2020>, 2020.

780 Lu, M. H., Chen, X., Liu, W. C., Zhu, F., Lim, K. S., McInerney, C. E., and Hu, G.: Swarms of  
781 brown planthopper migrate into the lower yangtze river valley under strong western pacific  
782 subtropical highs, *Ecosphere*, 8, <https://doi.org/10.1002/ecs2.1967>, 2017.

783 Lu, X., Hong, J., Zhang, L., Cooper, O. R., Schultz, M. G., Xu, X., Wang, T., Gao, M., Zhao, Y., and  
784 Zhang, Y.: Severe Surface Ozone Pollution in China: A Global Perspective, *Environ. Sci.  
785 Technol. Lett.*, 5, 487–494, <https://doi.org/10.1021/acs.estlett.8b00366>, 2018.

786 Lu, X., Zhang, L., Zhao, Y., Jacob, D. J., Hu, Y., Hu, L., Gao, M., Liu, X., Petropavlovskikh, I.,  
787 McClure-Begley, A., and Querel, R.: Surface and tropospheric ozone trends in the Southern  
788 Hemisphere since 1990: possible linkages to poleward expansion of the Hadley circulation,  
789 *Sci. Bull.*, 64, 400–409, <https://doi.org/10.1016/j.scib.2018.12.021>, 2019.

790 Ma, M., Yao, G., Guo, J., and Bai, K.: Distinct spatiotemporal variation patterns of surface ozone in  
791 China due to diverse influential factors, *J. Environ. Manage.*, 288, 112368,

792 <https://doi.org/10.1016/j.jenvman.2021.112368>, 2021.

793 Ma, Z., Xu, J., Quan, W., Zhang, Z., Lin, W., and Xu, X.: Significant increase of surface ozone at a  
794 rural site, north of eastern China, *Atmos. Chem. Phys.*, 16, 3969–3977,  
795 <https://doi.org/10.5194/acp-16-3969-2016>, 2016.

796 Maji, K. J., Ye, W. F., Arora, M., and Nagendra, S. M. S.: Ozone pollution in Chinese cities:  
797 Assessment of seasonal variation, health effects and economic burden, *Environ. Pollut.*, 247,  
798 792–801, <https://doi.org/10.1016/j.envpol.2019.01.049>, 2019.

799 Monks, P. S., Archibald, A. T., Colette, A., Cooper, O., Coyle, M., Derwent, R., Fowler, D., Granier,  
800 C., Law, K. S., Mills, G. E., Stevenson, D. S., Tarasova, O., Thouret, V., von Schneidemesser,  
801 E., Sommariva, R., Wild, O., and Williams, M. L.: Tropospheric ozone and its precursors from  
802 the urban to the global scale from air quality to short-lived climate forcer, *Atmos. Chem. Phys.*,  
803 <https://doi.org/10.5194/acp-15-8889-2015>, 2015.

804 Nie, J., Liu, P., and Zhao, C.: Research on Relationship between Various Indexes of the Western  
805 North Pacific Subtropical High and Summer Precipitation in Eastern China, *Chinese Journal*  
806 *of Atmospheric Sciences*, 45, 833–850, <https://doi.org/10.3878/j.issn.1006-9895.2009.20160>,  
807 2021.

808 O’Neill, B. C., Kriegler, E., Ebi, K. L., Kemp-Benedict, E., Riahi, K., Rothman, D. S., van Ruijven,  
809 B. J., van Vuuren, D. P., Birkmann, J., Kok, K., Levy, M., and Solecki, W.: The roads ahead:  
810 Narratives for shared socioeconomic pathways describing world futures in the 21st century,  
811 *Global Environmental Change*, 42, 169–180, <https://doi.org/10.1016/j.gloenvcha.2015.01.004>,  
812 2017.

813 Pu, B., Dickinson, R. E., and Fu, R.: Dynamical connection between Great Plains low-level winds  
814 and variability of central Gulf States precipitation, *J. Geophys. Res.*, 121, 3421–3434,  
815 <https://doi.org/10.1002/2015JD024045>, 2016.

816 Shen, L., Mickley, L. J., and Tai, A. P. K.: Influence of synoptic patterns on surface ozone variability  
817 over the eastern United States from 1980 to 2012, *Atmos. Chem. Phys.*, 15, 10925–10938,  
818 <https://doi.org/10.5194/acp-15-10925-2015>, 2015.

819 Silva, R. A., West, J. J., Zhang, Y., Anenberg, S. C., Lamarque, J. F., Shindell, D. T., Collins, W. J.,  
820 Dalsoren, S., Faluvegi, G., Folberth, G., Horowitz, L. W., Nagashima, T., Naik, V., Rumbold,  
821 S., Skeie, R., Sudo, K., Takemura, T., Bergmann, D., Cameron-Smith, P., Cionni, I., Doherty,  
822 R. M., Eyring, V., Josse, B., MacKenzie, I. A., Plummer, D., Righi, M., Stevenson, D. S., Strode,  
823 S., Szopa, S., and Zeng, G.: Global premature mortality due to anthropogenic outdoor air  
824 pollution and the contribution of past climate change, *Environ. Res. Lett.*, 8, 034005,  
825 <https://doi.org/10.1088/1748-9326/8/3/034005>, 2013.

826 Su, T., Xue, F., and Zhang, H.: Simulating the intraseasonal variation of the East Asian summer  
827 monsoon by IAP AGCM4.0, *Adv. Atmos. Sci.*, 31, 570–580, <https://doi.org/10.1007/s00376-013-3029-8>,  
828 2014.

829 Wang, Y., Jia, B., Wang, S. C., Estes, M., Shen, L., and Xie, Y.: Influence of the Bermuda High on  
830 interannual variability of summertime ozone in the Houston–Galveston–Brazoria region,  
831 *Atmos. Chem. Phys.*, 16, 15265–15276, <https://doi.org/10.5194/acp-16-15265-2016>, 2016.

832 Wu, D., Fung, J., Yao, T., and Lau, A.: A study of control policy in the Pearl River Delta region by  
833 using the particulate matter source apportionment method, *Atmos. Environ.*, 76, 147–161,  
834 <https://doi.org/10.1016/j.atmosenv.2012.11.069>, 2013.

835 Xu, W., Lin, W., Xu, X., Tang, J., Huang, J., Wu, H., and Zhang, X.: Long-term trends of surface  
836 ozone and its influencing factors at the Mt Waliguan GAW station, China-Part 1: Overall trends  
837 and characteristics, *Atmos. Chem. Phys.*, 16, 6191–6205, [https://doi.org/10.5194/acp-16-6191-](https://doi.org/10.5194/acp-16-6191-2016)  
838 [2016](https://doi.org/10.5194/acp-16-6191-2016), 2016.

839 Yan, M., Liu, Z., Liu, X., Duan, H., and Li, T.: Meta-analysis of the Chinese studies of the  
840 association between ambient ozone and mortality, *Chemosphere*, 93, 899–905,  
841 <https://doi.org/10.1016/j.chemosphere.2013.05.040>, 2013.

842 Yang, K., Cai, W., Huang, G., Hu, K., Ng, B., and Wang, G.: Increased variability of the western  
843 Pacific subtropical high under greenhouse warming, *Proc. Natl. Acad. Sci. U. S. A.*, 119,  
844 e2120335119, <https://doi.org/10.1073/pnas>, 2022.

845 Yihui, D., and Chan, J.: The East Asian summer monsoon: An overview, *Meteorology and*  
846 *Atmospheric Physics*, 89, 117–142, <https://doi.org/10.1007/s00703-005-0125-z>, 2005.

847 Yin, Z., Cao, B., and Wang, H.: Dominant patterns of summer ozone pollution in eastern China and  
848 associated atmospheric circulations, *Atmos. Chem. Phys.*, 19, 13933–13943,  
849 <https://doi.org/10.5194/acp-19-13933-2019>, 2019.

850 Zhan, Y., Luo, Y., Deng, X., Grieneisen, M. L., Zhang, M., and Di, B.: Spatiotemporal prediction of  
851 daily ambient ozone levels across China using random forest for human exposure assessment,  
852 *Environ. Pollut.*, 233, 464–473, <https://doi.org/10.1016/j.envpol.2017.10.029>, 2018.

853 Zhang, X., Jian, X., Zhao, Y., Liu, X., Chen, K., Wang, L., Tao, S., Liu, J., Huang, T., Gao, H., Liu,  
854 Y., Zhugu, R., and Ma, J.: Tropospheric Ozone Perturbations Induced by Urban Land  
855 Expansion in China from 1980 to 2017, *Environ. Sci. Technol.*, 56, 6978–6987,  
856 <https://doi.org/10.1021/acs.est.1c06664>, 2022.

857 Zhao, Z., and Wang, Y.: Influence of the West Pacific subtropical high on surface ozone daily  
858 variability in summertime over eastern China, *Atmos. Environ.*, 170, 197–204,  
859 <https://doi.org/10.1016/j.atmosenv.2017.09.024>, 2017.

860 Zhou, T., Yu, R., Zhang, J., Drange, H., Cassou, C., Deser, C., Hodson, D. L. R., Sanchez-Gomez,  
861 E., Li, J., Keenlyside, N., Xin, X., and Okumura, Y.: Why the Western Pacific subtropical high  
862 has extended westward since the late 1970s, *J. Clim.*, 22, 2199–2215,  
863 <https://doi.org/10.1175/2008JCLI2527.1>, 2009.

864